communications physics

ARTICLE

https://doi.org/10.1038/s42005-023-01361-3 OPEN

Active acoustic field modulation of ultrasonic transducers with flexible composites

Chenxue Hou[1,2,4], Zhaoxi Li[1,2,4], Chunlong Fei[1✉], Yi Li[1], Yecheng Wang[1], Tianlong Zhao[1], Yi Quan[1], Dongdong Chen[1], Xiaoping Li[2], Weimin Bao[2,3] & Yintang Yang[1✉]

The simple acoustic field generated by conventional transducers limits the development of ultrasound applications. Current methods rely on passive acoustic lenses or active arrays to manipulate ultrasonic waves, but they face challenges such as low transmission efficiency with bulky morphology for lenses, and complex systems with high-cost for arrays. Here, we propose a method exploiting flexible piezoelectric ultrasonic transducers (FPUT) with 1-3 PZT8/PDMS composites to achieve a high-frequency and diversified ultrasonic field. The FPUT at a center frequency of 1.5 MHz exhibits a high electromechanical coupling coefficient (k_t ~ 0.74), excellent transmission efficiency, and mechanical conformability. We showcase two dynamic functionalities of our setup, namely variable acoustic focus and multi-order vortex generated by circular and spiral shape transducers. Finally, we show that the FPUT achieves high-resolution underwater ultrasonic imaging at a wide spatial range (>12λ) via ultrasonic collimation, offering a viable technological alternative for active acoustic fields manipulation and ultrasonic applications.

[1] School of Microelectronics, Xidian University, 710071 Xi'an, China. [2] School of Aerospace Science and Technology, Xidian University, Xi'an, China. [3] China Aerospace Science and Technology Corporation, Beijing, China. [4] These authors contributed equally: Chenxue Hou, Zhaoxi Li. ✉email: clfei@xidian.edu.cn; ytyang@xidian.edu.cn

Ultrasonic transducers have the ability to convert electrical energy to mechanical energy related to the piezoelectric effect[1,2]. It is due to this property that ultrasound transducers are integrated into many devices and are used in a wide variety of applications, such as ultrasound imaging[3,4], acoustic tweezer manipulation[5], and focused ultrasound (HIFU) therapy[4–6]. Acoustic field modulation technology, especially beam steering, is a key element in facilitating the development of these applications. Acoustic field modulation technology plays an important role in many applications[7,8]. For example, in ultrasound imaging applications, acoustic waves focused is necessary because it can greatly improve the resolution of medical imaging and thus the quality of imaging. In HIFU applications, such as brain stimulation[9] and tissue ablation, the precision of the acoustic wave modulation will directly determine the effectiveness of the treatment, which requires the precise focusing of the acoustic waves at a defined location to treat a certain tissue area[10,11]. In the application of acoustic tweezers and drug delivery[12,13], acoustic waves can not only be focused and modulated to achieve the manipulation of individual particles but also to achieve vortex fields to accomplish the goal of particle or drug enrichment and targeted delivery[14]. In recent years, the rapid growth in demands for fine imaging and precise operation has led to the development of ultrasonic transducers characterized by higher frequencies, device flexibility, and diverse functions for the generation and modulation of complex acoustic fields.

The main methods of acoustic field modulation include the design of ultrasonic arrays[15,16] or the application of acoustic lenses[17,18]. The array can achieve real-time modulation of the ultrasonic acoustic field by modulating the excitation signal received by each array element and then completing the phase and amplitude modulation of the acoustic waves generated by the array elements, and ultimately realizing the real-time modulation of the desired acoustic field[19]. The array method, while innovative, faces several challenges. It is marked by high costs and a complex preparation process. Moreover, its functionality often depends passively on the specific shape of the object being measured. One of the main limitations of this method is its current low resolution, a result of having a restricted number of array elements. Achieving high-resolution acoustic field modulation across various spatial regions continues to be a significant hurdle. On the other hand, the passive way of acoustic lenses, including curved lenses[17], Fresnel lenses[20], holographic surfaces[21], metamaterial or metasurfaces[22], phononic crystals[23], etc. It has been shown that acoustic lenses can achieve high-resolution acoustic focused[23], acoustic vortex[24] and any complex acoustic field morphology, and even negative gradient refraction[25] and acoustic black holes[26]. The construction of the acoustic lens presents several challenges. The fabricated materials, coupled with the effects of acoustic coupling, can lead to an impedance mismatch between the lens and the piezoelectric element, as well as between the lens and the front propagation medium. This often results in poor energy transmission. Although existing additive manufacturing technology enables the production of parts with irregular and complex geometries, the limitations in process accuracy hinder the development of acoustic lenses for high-frequency, complex acoustic field modulation. Furthermore, the design constraint where the shape of the acoustic lens determines the distribution of the acoustic field means that each lens can only form a specific acoustic field. This inflexibility makes it challenging to meet the requirements for dynamic adjustment of the acoustic field and limits the reusability of the lenses. Besides the methods mentioned above, there still exists an active way to modulate the acoustic wave through the external force to make the piezoelectric material deformation to achieve the focus, vortex[27], etc., but this method will lead to the piezoelectric material broken, resulting in device robustness is reduced, and also the device is prepared to complete the inability to dynamically modulate the acoustic field.

Flexible piezoelectric materials offer a practical concept for acoustic field modulation. It has been shown that flexible devices have been successfully used in energy harvesters[28], wearable pressure sensors[29] spacecraft detection[30] and so on. Moreover, they have also been found suitable for utilization in the modulation of acoustic fields. Existing means of acoustic field modulation are based on rigid piezoelectric materials or non-bendable lenses, which cannot meet the requirements of diverse applications with anisotropic surfaces and dynamic generation of complex acoustic fields. The flexible feature allows customized modification of the geometry of the piezoelectric element to generate complex ultrasonic patterns without damaging the device and additional lenses. Flexible devices for various ultrasonic applications have been widely reported, and the preparation methods of flexible piezoelectric ultrasonic transducer (FPUT) can be broadly classified as follows. First, while the most straightforward and simple method is the deposition of piezoelectric thin films on flexible substrates using zinc oxide (ZnO)[31] and aluminum nitride (AlN) materials[32], the piezoelectric constants of such piezoelectric films are far from those of conventional lead zirconate titanate (PZT) piezoelectric ceramics. Second, piezoelectric polymers, such as polyvinylidene fluoride (PVDF) and its copolymers[33,34], are used as active materials for the fabrication of flexible ultrasonic devices. Due to their low electromechanical coupling coefficients and dielectric constants, the performance of the devices cannot meet the application requirements. Third, a composite structure is formed from elastic material and piezoelectric ceramic[35,36], a 1-3 composite structure is usually used to achieve high-piezoelectric performance[37]. The specific operation is to embed the piezoelectric ceramic pillar into the flexible matrix so that the device is locally rigid but overall flexible, with the advantages of both materials, to achieve high energy conversion efficiency and energy transmission efficiency.

In this work, we propose an active, flexible, and efficient acoustic field modulation based on the designed the FPUT at the center frequency of 1.5 MHz, which is composed of a flexible piezoelectric composite material (FPCM) with a 1–3 composite structure, as shown in Fig. 1a. The FPCM consists of PZT-8 and polydimethylsiloxane (PDMS) as the active and filler materials, respectively, to obtain sufficient sensitivity and flexibility. In addition, flexible electrodes with Ag and PDMS are attached to both sides of the 1–3 composites to provide sufficient conductivity and good acoustic matching for the transducer under bending conditions. As shown in Fig. 1b, this FPCM transducer realized by high-performance piezoelectric material, low modulus elastic material and stretchable interconnect structure design can be bent into specific shapes within a certain curvature range, which can modulate the radiation and propagation of the acoustic wave, and can realize real-time curvature adjustment to accomplish a series of frontier acoustic phenomena such as self-focusing and acoustic vortex. And based on the micro-injection pump operating system, the flexible and continuous deformation of the device is realized as shown in Fig. 1c, high-quality detection of object information at different spatial locations, such characteristics are of great significance to the research of medical imaging and industrial nondestructive testing applications.

Results and discussion

The array transducer provides a solution for generating efficient high-frequency ultrasonic waves and active ultrasonic fields, whereas the 3D-printed transmission hologram enables the miniaturization of low-frequency devices with unique

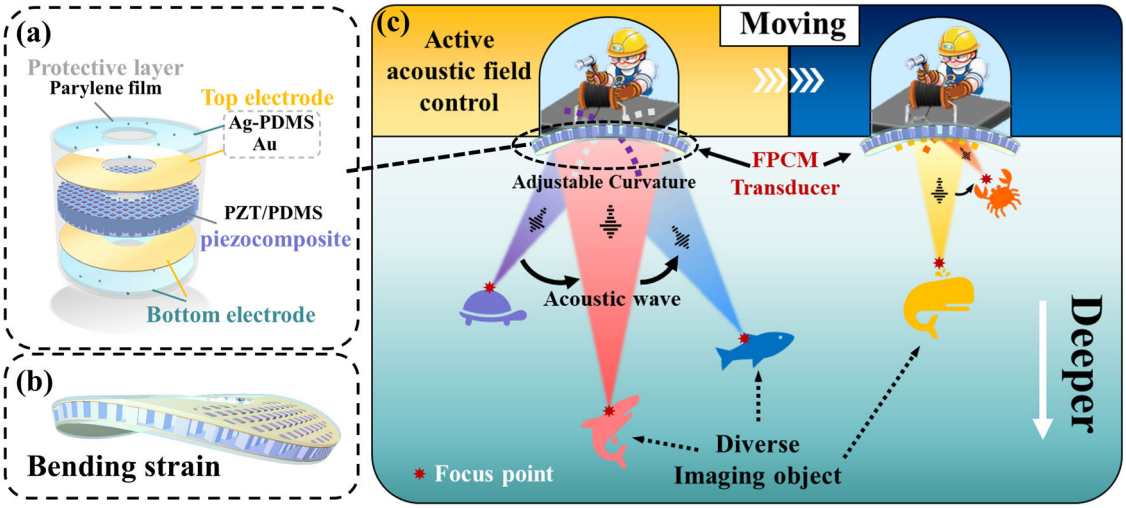

Fig. 1 Schematic diagram of the application of flexible transducers. a Detailed exploded-view schematic that summarizes the layout of the flexible piezoelectric ultrasonic transducers (FPUT) with lead zirconate titanate/polydimethylsiloxane (PZT/PDMS) composite. **b** Bending characteristics of devices. **c** Schematic diagram of a flexible device based on dynamic acoustic field modulation and its application to ultrasound imaging. For example, continuous zooming of a target object located at different spatial positions in a liquid environment and thus high-resolution ultrasound imaging is achieved.

functionalities. However, even for the formation of a simple focused acoustic beam, ultrasound arrays still require the excitation of a few hundred array elements with complex system operation. As for the acoustic hologram lens, the mismatch in acoustic impedance between the transducer surface (>30 Mrayls) and hologram (<3 Mrayls), along with internal losses within the hologram, leads to low efficiency in acoustic energy transmission, limiting practical ultrasound applications. To capitalize on the advantages of both technologies, we present a reliable method that combines them to achieve a high-frequency active and diversified ultrasonic field with high transmission efficiency in the water. Without acoustic lens and multi-element excitation, this is accomplished through the use of low acoustic impedance 3D flexible piezoelectric materials with sophisticated geometry. In our study, we modify the piezoelectric element's geometry to generate intricate ultrasound wave patterns that deviate significantly from conventional approaches. By changing the shape of FPCM, the phase distribution of the wavefront is reconstructed, and a variety of desired acoustic field patterns are formed, including dynamic focused and multi-order vortex acoustic fields. This method to reconstruct the phase distribution of wavefront is similar to the principle of acoustic holography. Moreover, the FPCM transducer, in contrast to the acoustic holograms, enables real-time, flexible changes in the morphology of the piezoelectric elements to create particular acoustic fields, which is useful for optimal acoustic field modulation for multi-focal dynamic imaging.

Preparation and characterization of FPCMs. As the active component of the transducer, the design principle of 1-3 FPCM is based on W.A.Smith theory[38]. The 1–3 composites have the advantages of high electromechanical coupling coefficient and low acoustic impedance, which will be conducive to energy transmission. The FPCM transducer takes thickness vibration as the main vibration mode and uses vibration displacement to represent its vibration mode, which further verifies the advantages of composites. The results are shown in Supplementary Materials, Fig. S1. PZT8 and PZT4 are commonly used "hard" as piezoelectric ceramic materials, and PZT8 is the best choice for resonant devices because of its better stability and higher electromechanical coupling coefficient. Figure 2a shows the electromechanical coupling coefficient (k_t) of 1-3 composites as volume fraction. Compared to conventional epoxy-matrix composites, PVDF and monolithic ceramic materials, this FPCM combines flexibility with a high electromechanical coupling coefficient. Based on the results with the finite element simulation model by COMSOL Multiphysics software, an FPCM with a frequency of 1.5 MHz is designed with a piezoelectric column width (pillar) and column spacing (kerf) of 500 μm and 200 μm, respectively, a volume ratio of 0.5, and a material thickness of 1.2 mm. The outer diameter of the FPCM is 30 mm and the inner diameter is 13 mm. A 2 × 2 matrix composed of four equally spaced piezoelectric pillars is regarded as a "unit". Because the 1–3 composite structure is periodic, the electrical and acoustic performance and vibration modes simulation of the FPCM is based on a unit, the results of which are shown in Fig. 2b. When describing vibration modes, the depth of color represents vibration displacement.

The preparation process of the whole device and the instruments used are shown in Fig. 2c. Regarding the electrodes of the device, we add an additional layer of soft conductive film on top of the gold plating to enhance the performance of the device. Therefore, here we choose a mixture of silver powder and PDMS to prepare the film, which can not only have good electrical conductivity but also can play a good acoustic impedance matching. The acoustic impedance of the composite piezoelectric material is 16.66MRayls. According to Desilets's theory[39] and the logarithmic model[40] of particle/polymer composite, the volume ratio of Ag-PDMS is 23.4% and the acoustic impedance of the conductive film is 3.35 MRayls[41]. For details, see the "Fabrication of the FPCM" subsection in the *Methods* Section. The physical and microscopic diagrams of the two electrodes are shown in Fig. 2d. Metallographic microscope images and Scanning Electron Microscope (SEM) images with a scale of 100 μm are used to show that the electrode quality is sufficient to give a good electrical connection to the device from the microscopic images. The impedance spectrum of the device with the two electrodes is shown in Fig. 2e. The Figure shows that the soft conductive clay film can significantly reduce the electrical impedance of the device and thus has better conductive characteristics. Besides, Fig. 2f demonstrates that it can still be stretched and twisted at high strain while maintaining high electrical conductivity. Finally, for the outer side of the FPCM, a protective film is applied for protection by vapor deposition in a vacuum environment, and the FPCM ultrasonic transducer is

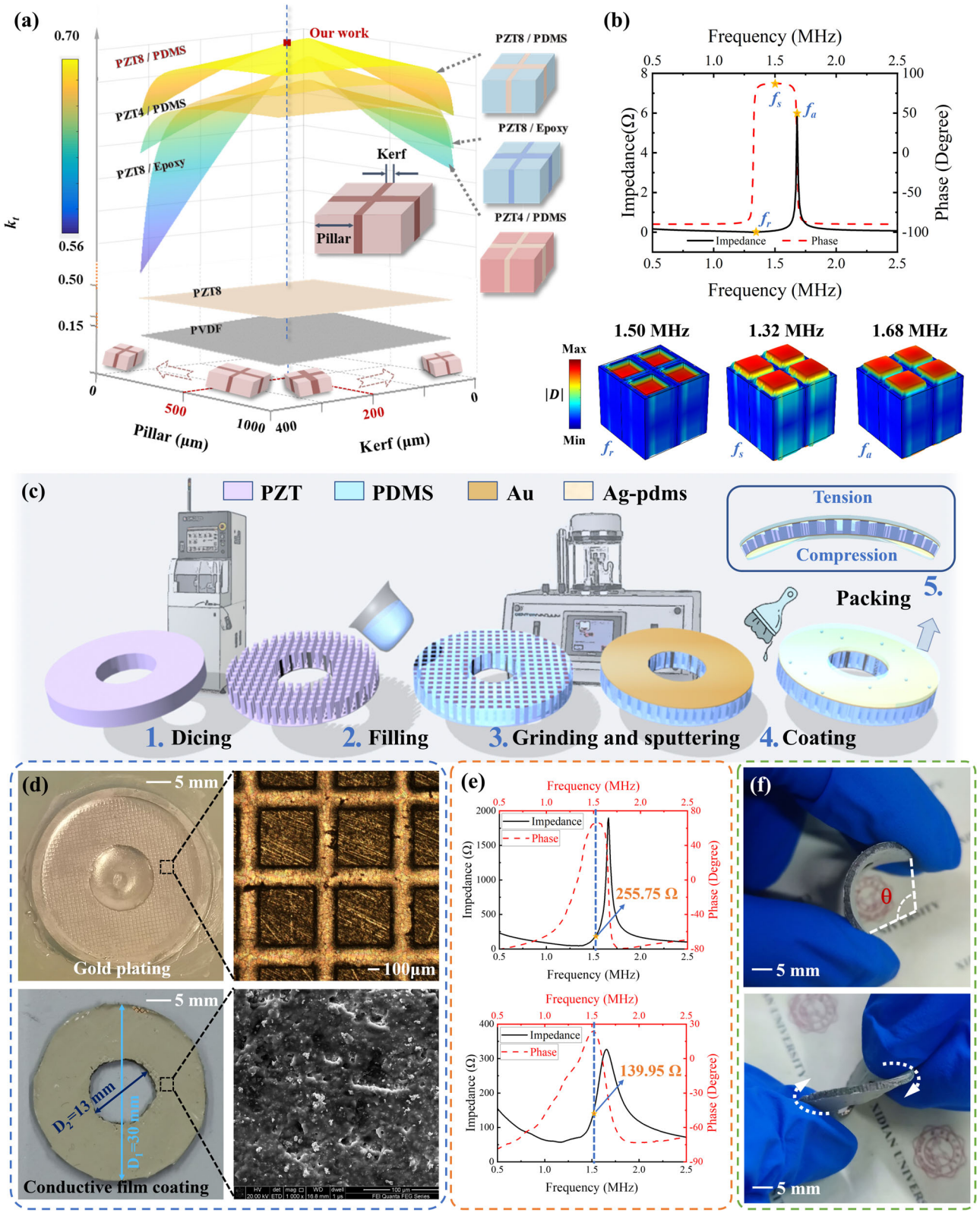

Fig. 2 Design and characterization of flexible transducers. a Comparison of electromechanical coupling coefficients (k_t) in three-dimensional form for transducers based on different composite materials, including lead zirconate titanate (PZT) series ceramics, polydimethylsiloxane (PDMS) and their composites. **b** Simulation of electrical and acoustic properties of transducers and vibration modes at vibration frequencies. Among them, the solid black line is the impedance spectrum, and the dotted red line is the phase spectrum. **c** Preparation process of the flexible piezoelectric composite material (FPCM) and transducers. **d** Metallographic microscope image of the transducer sputtered with the first electrode layers of gold, the SEM image of the transducer printed with the second electrode layers of Ag-PDMS. **e** Electrical and acoustic performance testing of transducers with two electrode layers, using the impedance analyzer. **f** Demonstration of transducer flexibility characteristics.

prepared regarding the device packaging guidelines[3,42]. Besides, in the same batch, three flexible devices with high performance were prepared, and their impedance spectra and performance results were summarized in Supplementary Materials, Fig. S2 and Table S2. The significant advantage of the FPCM transducer is its high electromechanical coupling factor (k_t-0.74), which implies that a larger proportion of the electrical input energy is effectively converted into mechanical output energy, leading to improved performance of the transducer.

Characterization of FPCM complicated acoustic field

Focusing acoustic field. We started with an FPCM transducer to achieve acoustic focusing at different depths of focus. The left part of Fig. 3a shows the distribution of the theoretical focal length of the transducer, from which, it can be seen the device based on FPCM with dynamic variable curvatures can converge the generated acoustic beams to different circular focal positions. This feature is verified based on 3D finite element analysis (FEA) simulations with COMSOL Multiphysics software. As shown in the right of Fig. 3a, the simulated acoustic field in the xz plane demonstrates the active performance of focusing energy at different focal depths. As the radius of curvature (R_c) of the FPCM ranges from 17.5 mm to 30 mm, the focal position of the focused acoustic beam changes from 11.45 mm to 26.32 mm, showing multi-focus properties. The contours of the acoustic field focus areas formed by different R_c are extracted and combined together, using the plane where the device surface is located as the z-axis as the unified origin. The comparison shows that as the R_c increases, the more the device tends to be flat, the focus position is gradually farther away, and the available focus area is wider. As shown in Fig. 3b, when the xy plane is intercepted at the focal point of the acoustic field at different R_c respectively, the acoustic field still exhibits the focusing feature with different acoustic beam widths.

More data were extracted from the test results and processed, and the quantitative results were plotted in Fig. 3c–e. The conventional transducer is the reference group, referring to the flat ultrasonic transducer of the same size. As shown in Fig. 3c, the uniqueness of our designed FPCM transducers compared to conventional ultrasound transducers lies in their ability to achieve excellent collimation results, which is a significant point in ultrasound imaging applications. In addition, the full width at half maximum (FWHM) is used to evaluate the imaging resolution[43]. The explanation of the FWHM is shown in the Supplementary Materials, Fig. S4. As a result, the range of lateral resolution variation at the focal position is 0.79–1.21 mm, and the range of axial resolution variation is 4.45–14.01 mm, The specific calculation results are shown in Table S1 of Supplementary Information. The above phenomenon shows that the device can achieve high-resolution dynamic imaging in a large space range. With the increase of R_c, its resolution decreases, but it is still higher than that of the planar transducer. From the result in Fig. 3d, e, it can be analyzed that the smaller the width of the acoustic beam will obtain the higher resolution, thus proving the highest resolution with a R_c of 17.5. Moreover, the -6dB lateral acoustic field resolution increases from 0.78 mm to 1.55 mm as the depth of focus becomes progressively larger. Figure 4a, b illustrates the conceptual diagram and a flow schematic of the acoustic field measured setup. The specific test installation and process of the acoustic field are shown in the "Test of acoutic field morphology" subsection in the Methods section. The cross-sections of the xy and xz planes at the focal position are used to represent the characteristics of the focused acoustic field[44]. As shown in Fig. 4c, the measured acoustic fields with a radius R_c of 17.5 mm and 30 mm clearly demonstrate the active ultrasonic focused characteristics, and the focal lengths of the focused acoustic fields obtained for the two R_c are 11.94 mm and 26.23 mm, respectively. In summary, it is shown to be consistent with the above FEA simulation results (focal lengths of 11.01 mm and 24.28 mm in the acoustic field simulation results, respectively). Figure 4c shows that the FPCM transducer with a radius of 30 mm has a larger focused area and a wider range of operations. In addition, it is worth noting that the measured pressure distribution is not completely symmetrical, and there is a small deflection in the acoustic field measured results. This is mainly due to the random gap between the FPCM transducer and the mold, which makes the deformation formed by the transducer not complete to reach the theoretical curvature. Moreover, some unavoidable artificial error factors are introduced in the process of acoustic field measurement. Because the experiment was done manually.

Vortex acoustic field. In order to verify more functions of ultrasonic field modulation, a flexible spiral transducer was designed using FPCM and used to achieve the focused vortex beam with different focus points and topological charge. Figure 5a illustrates the key parameters of the FPCM transducer. Consider a complete ring with an angle spanning from 0 to 2π. As shown in Fig. 5a, one side of the FPCM ring is cut radially, and the cut mark is in the PDMS region. This step is simple but irreversible. With that, the spiral ring is sequentially fixed in 3×3D printing molds of different orders designed to form the required spiral shape and the mold is designed with slots on both the inner ring and the outer ring, so that the transducer is pressed tightly to the mold. The drawing of 3D printed mold with a slot is shown in the Supplementary Materials, Fig. S5. The vertical offset of the upper surface at both ends of the FPCM ring is denoted by H. The height H is set to 2 mm, 3 mm, and 4 mm, which is calculated by multiplying the wavelength (λ) of acoustic wave propagating in water with this frequency and the order (n), where $n = 2,3,4$[45].

Experimental devices and measured principles are shown in the *Methods* section of "Test of acoustic field morphology". The scanning area of the xy plane is 10 mm × 10 mm and the xz plane is 40 mm × 22 mm, and the step size is 100 μm. Figure 5b displays the measured results of pressure amplitude distribution in the x–z plane. When H is 2,3,4, the measured results of the maximum acoustic pressure of the vortex acoustic field in the three groups are 2.35,1.932 and 1.62 MPa, respectively. In order to show the characteristics of the acoustic field more clearly, each group was normalized with the maximum acoustic pressure as the standard value, respectively. It can be seen from the acoustic field test results that different from the focused acoustic field, different vertical offset H cannot only change the topological order of the vortex field but also affect the depth of focus. As the vertical offset H changes from 2 mm to 3 mm and 4 mm, the depth of focus increases from 16 mm to 17 mm and 18 mm. It seems that the emitted ultrasound waves appear to converge in the direction of propagation. The 3D structure of the acoustic intensity distribution was created by combining the acoustic field intensity distributions of the x–y plane at various depths in order to create a more understandable acoustic field intensity distribution, as shown in Fig. 5c. From the measured acoustic field distributions of the three manipulation groups, it is seen that the region of maximum acoustic pressure is expanding as the height offset increases; Moreover, in the phase diagram, with the increase of height offset, the phase achieves the second-, third-, fourth-order features, respectively. The order here refers to several cycles of 0 to 2π changes in phase in the range of directional angles 0 to 360°. Figure 5c shows amplitude on the left and phase distribution on the right. In the z-axis direction, the inner ring acoustic pressure of the vortex acoustic field increases first and then decreases, indicating that the acoustic field has obvious convergence

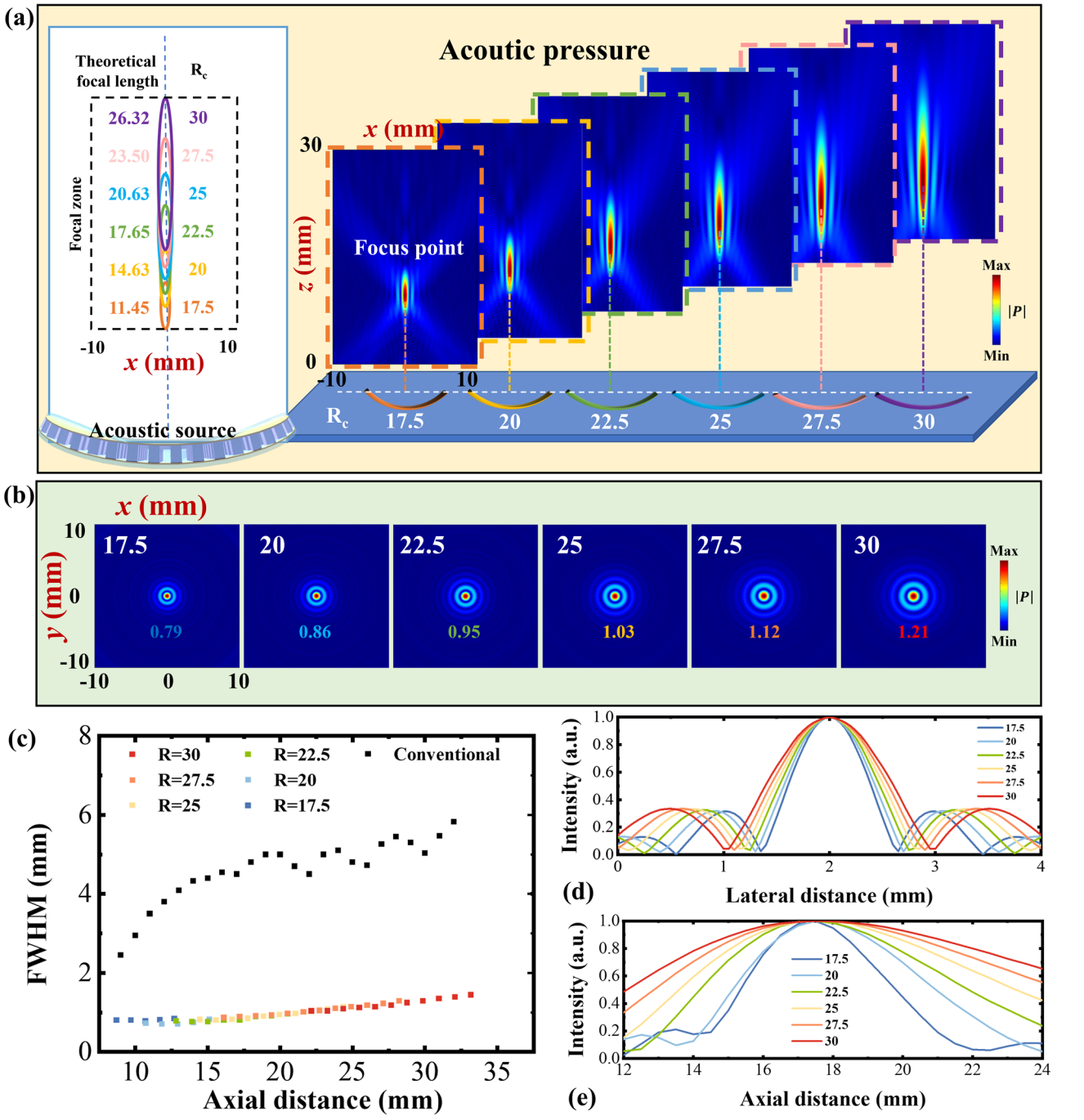

Fig. 3 3D FEA simulation of acoustic field morphology and spatial location of the transducer produced at different radii of curvature. a In the *xz* plane, the theoretical focused zone and simulated focused acoustic field corresponding to different radius of curvature (R_c) on the same *x*-axis are obtained. **b** The *xy* plane distribution of the focused acoustic field corresponding to six different R_c is shown, with a cross-sectional area of 10 × 10 mm^2. **c** Collimation characteristics of the acoustic field: The colored and black dashed lines show the full width at half maximum (FWHM) values of our prepared transducer and the conventional flat transducer at different axis distances. **d** Lateral resolution of the acoustic field corresponding to different R_c. **e** Longitudinal resolution of the acoustic field corresponding to different R_c.

characteristics. Figure 5d is a partial enlargement of Fig. 5c, which more clearly characterizes the measured acoustic field, the top line shows the phase distribution of the acoustic pressure, which is distributed periodically, extracting the annular data at a radius of 5 mm, indicating that in the angular range from 0 to 360°, the phase of the acoustic field shows an *n*th order distribution, and the corresponding fold line with n complete -π to π variation periods. The acoustic pressure amplitude in the following row is distributed in a circular pattern, with the highest acoustic pressure in the circular line at the position closest to the center of the circle, which is the highest point in the curve. The purple dotted line converges the experimental measurements of the amplitude corresponding to the different x-direction positions, and the results of the fit are shown in the orange curve. The spacing between the two highest points increases as R_c increases. In addition, the characterization of acoustic field and radiation force for the spiral FPCM transducer at different vertical offset (H) is added to prove that the transducer can generate sufficient

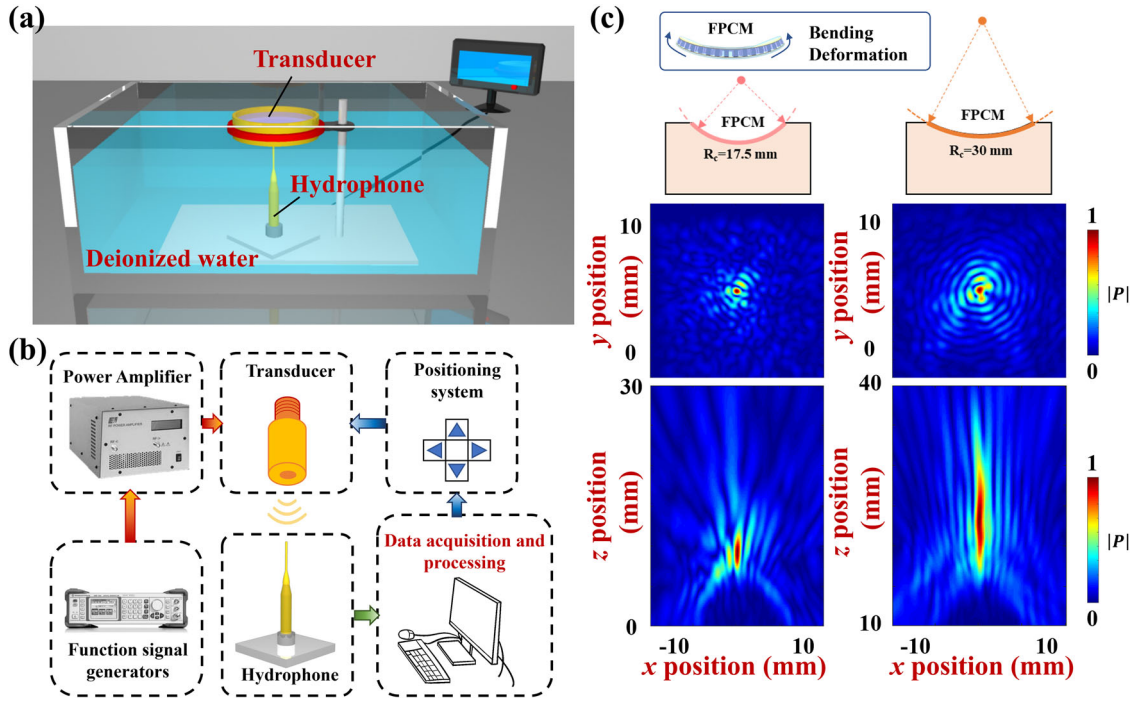

Fig. 4 Measurement of acoustic field morphology and spatial position generated by the transducer at different radii of curvature. a Schematic diagram of the measurement environment and installation. **b** Construction of the measurement system. **c** Acoustic field measurement of flexible piezoelectric composite (FPCM) transducers with a radius of curvature of 17.5 mm and 30 mm respectively.

forces for manipulation applications. Corresponding simulation results have been added in the Supplementary Materials, Fig. S6. Simulation results show that the magnitude of the exerted radiation force, spanning several nN to pN[12,46], is adequately substantial for particle manipulation. Through the above experiments, it is verified that the desired vortex beam can be simply customized by modifying the three-dimensional spatial structure of the FPCM, which enriches the distribution form of the acoustic field and modulation applications.

Dynamic multifocal imaging. Ultrasound imaging is a radiation-free, non-invasive method that has been widely used in clinical diagnosis and treatment in recent years. Conventional focused single-element transducers have a limited focusing area, while the arrays are expensive and complex to operate. To more visually demonstrate the advantages of the designed FPCM transducer, the high-quality ultrasound imaging is shown with the active acoustic field manipulation over a large spatial range. We simulated ultrasound imaging for detecting unidentified objects at different depths inside the human body, here we use a 3D printed high-precision stepped digital plate to simulate the object to be measured and embedded inside the agar phantom, the details are shown in Supplementary Materials, Fig. S7. Agar tissue phantoms have served as adequate human tissue substitutes for the evaluation of ultrasound imaging and other effects. The digital plate is made of photosensitive resin material and is used to simulate diseased tissue or implanted objects inside human tissue. The details of the phantom are shown in the "Preparation of phantom" subsection in the *Methods* section.

We assembled a multi-focus FPCM transducer and microinjection pump operating system (Voyaging Power Formula, Model QHSS-001A, China) that can dynamically adjust the R_c on the basis of the annular FPCM prepared, and detected objects at different focal positions by varying the curvatures. This flexibility makes it possible for the research instrument to image objects at different depths that are inside the obstruction in a non-contact mode, with R_c variations from 17.5 mm to 27.5 mm. Figure 6a, b shows a schematic and realistic view of the experimental setup. A photograph of the microinjection pump system is shown in Supplementary Materials, Fig. S8.

We respectively adopted five kinds of the curvature radii to form the focal zone with different depths, so that each acoustic beam was concentrated on the surface of the digital plate. Figure 6a shows the setup with dynamically varying R_c. With the aid of a microinjection pump, specifically, converting the stretching distance of the syringe to R_c, so that the R_c of the controlled device can be set precisely and automatically and the currently set R_c can be read visually. Where, the flexible piezoelectric composite is fixed at the outer diameter and stretched by the syringe in the radial backward direction inside the center to form the specified curvature and maintained. What's more, five different R_c were selected for imaging experiments. The specific dimensions of the digital plate used are as follows: The height of each step is 7 mm, the cross-sectional area was 25 mm × 25 mm, and the height difference between the two adjacent steps was 3 mm. The R_c of the transducer is continuously adjusted so that the focus of the transducer is located at the focus position of the five steps respectively, with R_c of 17.5,20,22.5,25, and 27.5 mm. Specifically, the transducer is immersed in water and as close to the agar surface as possible to ensure that the object to be measured is located in the focal zone.

Constant depth mode (C mode) is used to obtain ultrasound imaging images. Specifically, the FPCM transducer is connected to Pulser/Receiver (DPR500, Imaginant, Pittsford, NY, USA), which is used to transmit and receive pulse signals, and then the received signals to the self-built ultrasound imaging system for post-processing. Scanning step size of x-axis is 4 μm, and the scanning step size of y-axis is100μm, the time window to analyse data is 10–30 μs. Then the ultrasound imaging results are shown in Fig. 6c, where the available imaging range becomes wider as the R_c deepens, which further validates the simulation conclusions presented in Fig. 3. In addition, the signal on the central axis

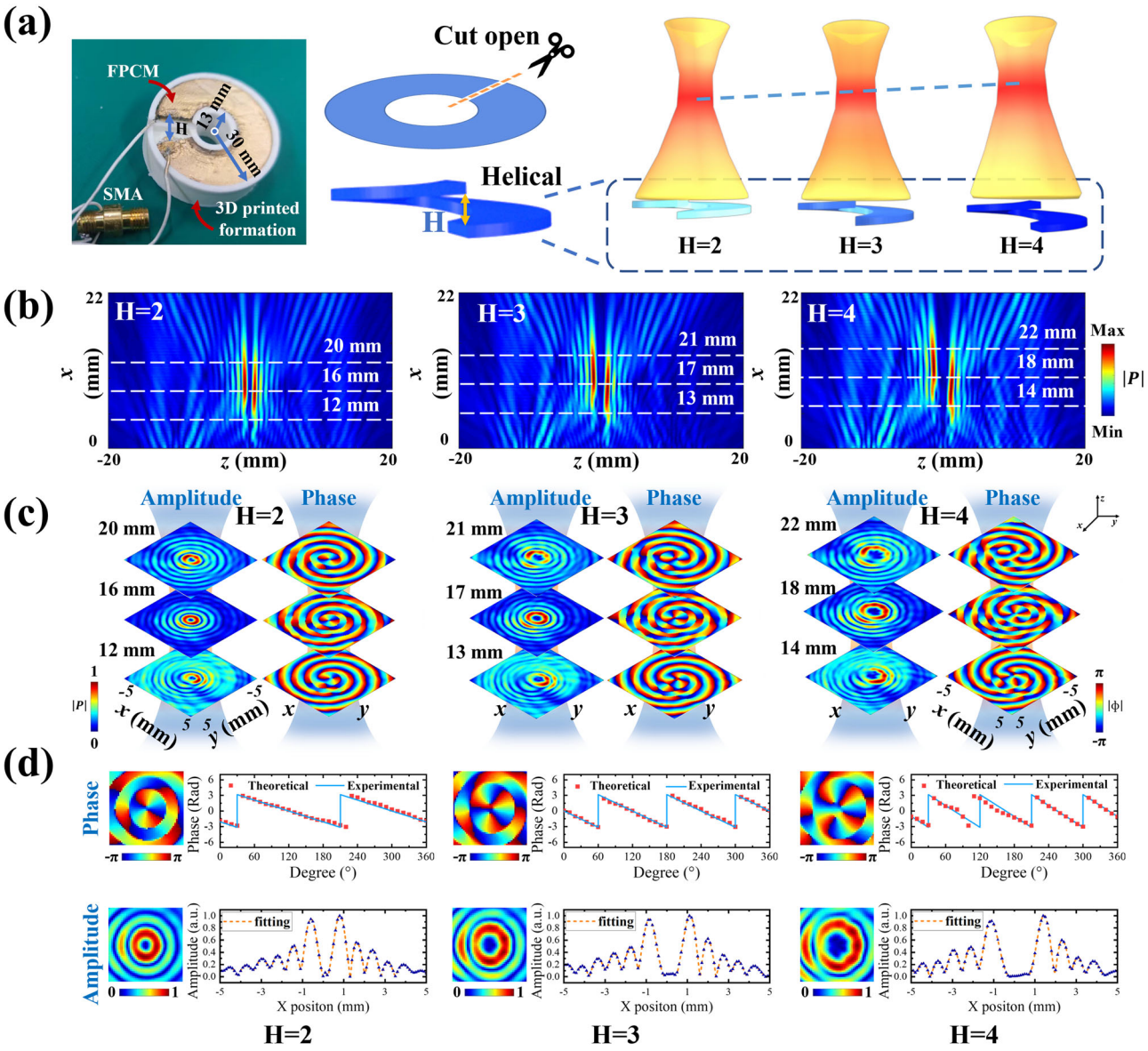

Fig. 5 Measured results of vortex acoustic field generated by transducer at different radius of curvature. a The assembly process of the flexible piezoelectric composite material (FPCM) transducer for the formation of the vortex acoustic field: the different vertical offset (H) values is 2 mm, 3 mm and 4 mm. **b** Results of the acoustic field test in xz-plane. **c** The measured results of the acoustic field in the xy-plane at the position marked by the white dashed line in (**b**) are shown. **d** Quantification of acoustic field characteristics in terms of phase and amplitude distribution of the acoustic field: the blue dash and red dotted line represent the experimental measurement and theoretical value of the phase distribution; the purple dotted line represents the experimental measurement of amplitude distribution and the orange curve is the fitting results.

(marked by the red dashed line) of the imaging image is extracted for data processing, and the intensity distribution is shown in Fig. 6d. The distribution with low amplitude in the intensity map corresponds to the spatial location of the skeletonized part for the digital plate, and conversely, the high amplitude represents that the acoustic waves are heavily reflected at the digital plate interface.

In conclusion, we validated that the FPCM transducer has the capability of non-contact dynamic focus imaging over a wide spatial range(å 12λ, λ is the wavelength of the acoustic wave in the phantom, and the acoustic velocity of phantom is about 1450 m/s). This dynamic focusing capability is fundamentally different from that of conventional focused single-element transducers. To expand, the focus zone of a conventional single-element transducer is directly related to its focal length, and although it can broaden the focus zone by adjusting the focal length, complex application scenarios often do not allow it to do so. Therefore, the FPCM transducer provides a significant improvement in device performance and operational continuity and convenience. These advantages provide a solution for the non-destructive ultrasound detection of objects to be measured in the interior and could be applied in the future to detect malformations or cancerous tissues in human tissues.

Conclusion

In order to meet the requirements and difficulties of numerous applications, including in vivo drug delivery, and in vivo imaging, for dynamically tunable complex acoustic fields and non-contact manipulation environments, this paper designs an ultrasonic transducer with high-performance FPCM as piezoelectric elements, flexible conductive plasma film as the electrodes for dynamic multi-focus ultrasound imaging. The prototype

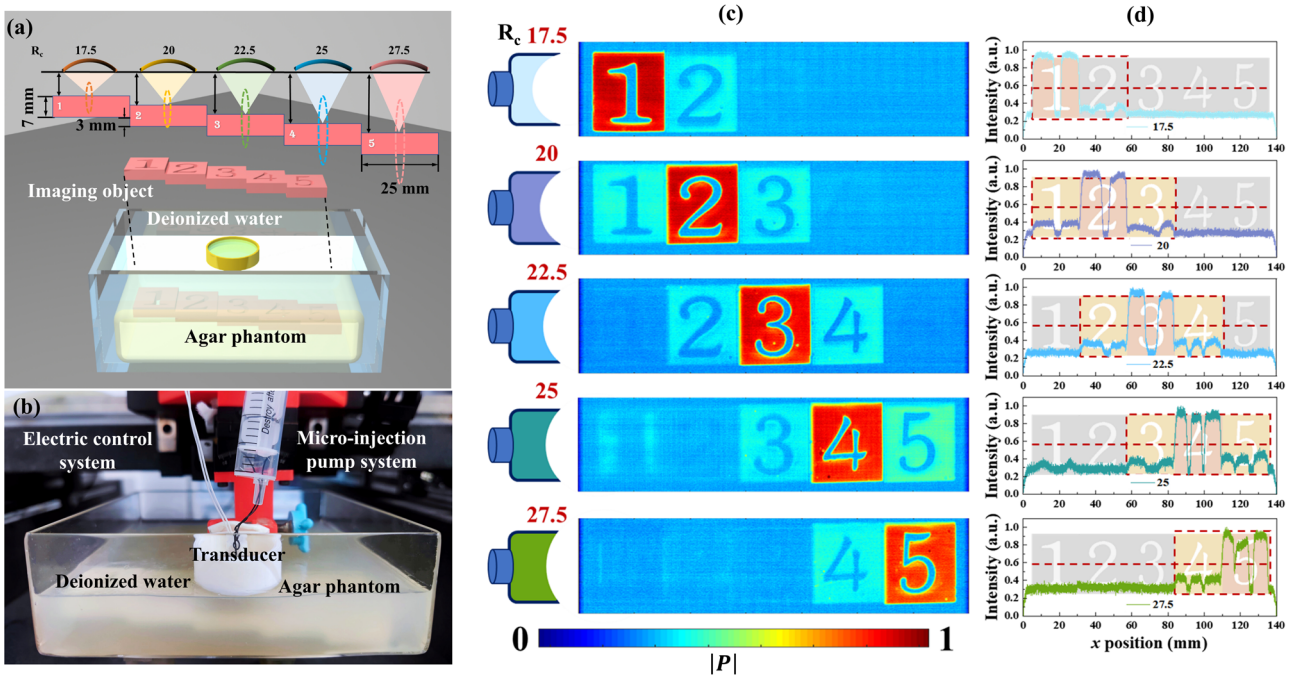

Fig. 6 Experimental implementation of dynamic acoustic field modulation. a Schematic diagram of the experimental device includes the size of the digital plate (imaging object) and the principle of dynamic multifocal imaging with the transducer at different curvatures. **b** Photogram of the experimental setup. **c** Ultrasound imaging of digital plates based on continuous dynamic adjustment method. **d** Signal extraction and analysis of ultrasound imaging results.

transducer exhibits strong mechanical flexibility and adequate acoustic performance in terms of frequency (~1.51 MHz) and electromechanical coupling coefficient ($k_t \sim 0.74$). In order to achieve different acoustic field styles, we designed two kinds of ultrasonic transducers, circular transducers and spiral transducers, based on FPCM, in which FPCM can be customized to bent into a specific shape within a certain limit, thanks to the design of this low modulus elastic material and stretcher structure.

Based on the above advantages, the device can realize acoustic wave modulation, and achieve a series of acoustic field morphologies such as real-time curvature adjustment, complete self-focusing, and acoustic vortex. The focusing and vortex effects of the FPCM transducer were also verified by scanning the x–y and x–z plane with a hydrophone. As well, C-mode ultrasound imaging of objects located at different depths within the agar model was achieved for non-contact dynamic multifocal imaging experiments, validating the profound application value of this feature. The above results indicate that the designed transducers can achieve outstanding performance in flexibility and sensitivity for transducer applications.

Although the device is currently unable to achieve the patterned and complex acoustic field distributions of thousands of pixel design, the study demonstrates its potential as a practical method for active manipulation of acoustic fields by enabling dynamic focusing acoustic fields for ultrasonic imaging applications and high-order topological vortex beam acoustic fields for acoustic tweezers with radiated shear forces.

In our future work, we plan to further optimize this approach in two ways: first, to improve the flexibility and piezoelectric properties of the device, so that it can achieve high-resolution acoustic fields with higher pixel densities. Secondly, the bonding method of PDMS by chemical means is studied, so that the cut FPCM can be restored and the reuse rate of the device can be improved. In a word, combined with the above optimization methods, ultrasonic transducers are expected to be optimized in the direction of miniaturization, integration, and reuse. Based on the above characteristics, acoustic field manipulate will obtain more excellent application effects in more fields.

Methods

Fabrication of the FPCM. Figure 1b presents a detailed exploded-view schematic that summarizes the layout of the flexible transducer. The annular shape of the transducer is more convenient for deformation, and it is easier to fix the deformation of the transducer. When designing the vortex acoustic field, it can easily achieve the formation of helical-like structure. The FPCM consists of three parts: the flexible composites, the flexible electrode, and the protective layer. The manufacturing process of the flexible 1-3 composite transducer and the instrumentation used for the process are shown in Fig. 4. Based on the simulated design parameters, 1-3 PZT-8/PDMS composites were fabricated using the "dice and fill" method[47]. The PZT-8 ceramics were cut in both directions using a 200 μm thick dicing saw (diamond blade, DISCO). The cut ceramics were pretreated using ultrasonic and plasma cleaning method, which can enhance the adhesion between the PZT-8 ceramic surface and the cured PDMS. Liquid PDMS (Sylgard 184, Dow Corning) was then filled into the cutting tank using a 10:1 weight ratio using a spin coating technique and then cured at a temperature of 100° for 30 min. By grinding the surface of the sample until the piezoelectric pillar is exposed, then the gold electrode layer is plated on both sides of the sample surface by vacuum sputtering method and coated with a flexible conductive film. The silver powder doping fraction is determined by combining Desilets's theory and the logarithmic model of particle/polymer composite with the following calculation:

$$Z_m = \sqrt[3]{Z_P Z_F^2}$$

where the Z_m represents the acoustic impedance of the conductive matching layer, Z_p is the piezoelectric material is acoustic impedance, and Z_F is the front-end propagation medium acoustic impedance, here is water. The acoustic impedance of the composite piezoelectric material is 16.66 MRayls. According to Desilets's theory, the acoustic impedance of the flexible conductive film is 3.35 MRayls. In order to achieve a good acoustic impedance match, the silver powder volume ratio of the flexible conductive film is set to

23.4% based on the logarithmic model of particle/polymer composite. And the design principle of one-quarter wavelength matching is adopted, the film thickness is about 110 μm. For subsequent immersion experiment in water, a protective film, approximately 3um thick, is deposited on the overall surface of the device using *parylene C* material. Finally, the transducer is electrically connected using a coaxial cable, where the ends of the coaxial cable are connected to the electrodes of the transducer and the SMA (SubMiniature version A) converter respectively.

Characterization of FPCM device. In order to test the performance of the designed FPCM device, a series of classical electrical and acoustic tests are performed. As shown in Fig. 2e, electric impedance and phase characteristics were characterized with an impedance analyzer (Wayne Kerr Electronics, UK). In order to test the effect of conductive film as the electrode layer on the performance of the device, the test devices were coated with Au electrode layer and conductive film, respectively. From the above electrical test results, it can be seen that the center frequency is 1.55 MHz and 1.51 MHz, and the impedance at the resonant frequency is 255.75 Ω and 139.95 Ω. The results show that printing a conductive film after Au plating leads to a significant decrease in the resistance of the device at the resonant frequency, demonstrating a significant improvement in the electrical performance of the device. Besides, the encapsulated transducer has a high electromechanical coupling coefficient of 0.74. Moreover, the transducer still maintains high electrical and acoustic performance with different curvatures. Electrical and acoustic performance measurements under different curvature conditions are shown in Supplementary Materials, Fig. S3.

Test of acoutic field morphology. The acoustic field test and characterization relies on the detection principle of single transmission and receive of acoutic waves. The acoustic waves emitted by the designed FPCM transducer are received by a high-performance hydrophone. The FPCM transducer is driven by the function signal generator (Rohde & SCHWARZ, SMB 100A) that generates a continuous wave with the center frequency, with which the signal is amplified using a power amplifier (Electronics & Innovation, 525LA). A needle hydrophone (NH1000, Precision Acoustics, Dorchester, UK) is fixed at the bottom of the water tank which is filled with deionized water. Using a 3D motion system, the FPCM transducer position is adjusted so that the transducer center is aligned with the hydrophone and in the focal position. Then, A with a step size of 100 μm is controlled by the computer to obtain 2D distribution of acoustic pressure. The received ultrasound signals are recorded through the capture card and the data processing of the matrix is performed using Labview software.

Preparation of phantom. We use a 3D-printed high-precision digital plate embedded in an agar phantom[48] to simulate unidentified objects inside the human body at different depths and to perform ultrasound imaging of them. The digital plate was placed horizontally in glassware with effective mechanical support, close to the bottom of the vessel. Weighed agar powder was poured into boiling water, stirred well, and gently poured into the glassware when the suspension became translucent, and then left for 12 h to solidify. The specific parameters of the digital plate are as follows: the thickness of each step is 7 mm, the height difference between adjacent steps is 3 mm, and the total thickness of the digital plate is 19 mm.

Data availability

The authors declare that the data supporting the findings of this study are available within the paper and its supplementary information files.

Received: 5 March 2023; Accepted: 28 August 2023;
Published online: 15 September 2023

References

1. Zhou, Q. et al. Piezoelectric single crystal ultrasonic transducers for biomedical applications. *Prog. Mater. Sci.* **66**, 87–111 (2014).
2. Shung, K. K., Cannata, J. M. & Zhou, Q. Piezoelectric materials for high frequency medical imaging applications: a review. *J. Electroceram.* **19**, 141–147 (2007).
3. Li, Z. et al. Coding piezoelectric metasurfaces. *Adv. Funct. Mater.* **32**, 2209173 (2022).
4. Wang, C. et al. Bioadhesive ultrasound for long-term continuous imaging of diverse organs. *Science* **377**, 517–523 (2022).
5. Li, J. et al. Three dimensional acoustic tweezers with vortex streaming. *Commun. Phys.* **4**, 1–8 (2021).
6. Beisteiner, R. et al. Transcranial pulse stimulation with ultrasound in Alzheimer's disease—a new navigated focal brain therapy. *Adv. Sci.* **7**, 1902583 (2020).
7. Ma, Z. et al. Acoustic holographic cell patterning in a biocompatible hydrogel. *Adv. Mater.* **32**, e1904181 (2020).
8. Baudoin, M. et al. Folding a focalized acoustical vortex on a flat holographic transducer: Miniaturized selective acoustical tweezers. *Sci. Adv.* **5**, eaav1967 (2019).
9. Zhang, T. et al. Piezoelectric ultrasound energy-harvesting device for deep brain stimulation and analgesia applications. *Sci. Adv.* **8**, eabk0159 (2022).
10. Illing, R. O. et al. The safety and feasibility of extracorporeal high-intensity focused ultrasound (HIFU) for the treatment of liver and kidney tumours in a Western population. *Br. J. Cancer* **93**, 890–895 (2005).
11. Beisteiner, R. & Lozano, A. M. Transcranial ultrasound innovations ready for broad clinical application. *Adv. Sci.* **7**, 2002026 (2020).
12. Ozcelik, A. et al. Acoustic tweezers for the life sciences. *Nat. Methods* **15**, 1021–1028 (2018).
13. Lajoinie, G. et al. Non-spherical oscillations drive the ultrasound-mediated release from targeted microbubbles. *Commun. Phys.* **1**, 1–9 (2018).
14. Li, Z. et al. The forbidden band and size selectivity of acoustic radiation force trapping. *iScience* **24**, 101988 (2021).
15. Hu, H. et al. Stretchable ultrasonic transducer arrays for three-dimensional imaging on complex surfaces. *Sci. Adv.* **4**, eaar3979 (2018).
16. Wang, C. et al. Continuous monitoring of deep-tissue haemodynamics with stretchable ultrasonic phased arrays. *Nat. Biomed. Eng.* **5**, 749–758 (2021).
17. Melde, K., Mark, A. G., Qiu, T. & Fischer, P. Holograms for acoustics. *Nature* **537**, 518–522 (2016).
18. Marzo, A. et al. Holographic acoustic elements for manipulation of levitated objects. *Nat. Commun.* **6**, 8661 (2015).
19. Cannata, J. et al. Development of a 35-MHz piezo-composite ultrasound array for medical imaging. *IEEE Trans. Ultrason Ferroelectr. Freq. Control* **53**, 224–236 (2006).
20. Tarrazó-Serrano, D. et al. Design of acoustical bessel-like beam formation by a pupil masked soret zone plate lens. *Sensors* **19**, 378 (2019).
21. Marzo, A. & Drinkwater, B. W. Holographic acoustic tweezers. *Proc. Natl Acad. Sci. USA* **116**, 84–89 (2019).
22. Liao, G. et al. Acoustic metamaterials: a review of theories, structures, fabrication approaches, and applications. *Adv. Mater. Technol.* **6**, 2000787 (2021).
23. Li, Z. et al. Focus of ultrasonic underwater sound with 3D printed phononic crystal. *Appl. Phys. Lett.* **119**, 073501 (2021).
24. Shen, L. et al. Self-stabilizing three-dimensional particle manipulation via a single-transducer acoustic tweezer. *Appl. Phys. Lett.* **122**, 094106 (2023).
25. Xie, Y. et al. Wavefront modulation and subwavelength diffractive acoustics with an acoustic metasurface. *Nat. Commun.* **5**, 5553 (2014).
26. Fu, Y. et al. Compact acoustic retroreflector based on a mirrored Luneburg lens. *Phys. Rev. Mater.* **2**, 105202 (2018).
27. Chen, X. et al. Helical-like 3D ultrathin piezoelectric element for complicated ultrasonic field. *Adv. Funct. Mater.* **29**, 1902912 (2019).
28. Jiang, L. et al. Flexible piezoelectric ultrasonic energy harvester array for bio-implantable wireless generator. *Nano Energy* **56**, 216–224 (2019).
29. Hong, Y. J. et al. Wearable and implantable devices for cardiovascular healthcare: From monitoring to therapy based on flexible and stretchable electronics. *Adv. Funct. Mater.* **29**, 1808247 (2019).
30. Lü, X. et al. Numerical and experimental investigation of aerodynamic heat control of leading edge of hypersonic vehicle's flexible skin. *Sci. China Inf. Sci.* **65**, 202203 (2022).
31. Zhou, X. S. et al. Sputtered ZnO film on aluminium foils for flexible ultrasonic transducers. *Ultrasonics* **54**, 1991–1998 (2014).
32. Fei, C. et al. AlN piezoelectric thin films for energy harvesting and acoustic devices. *Nano Energy* **51**, 146–161 (2018).

33. Su, Y. et al. Piezoelectric textiles: muscle fibers inspired high-performance piezoelectric textiles for wearable physiological monitoring. *Adv. Funct. Mater.* **31**, 2170136 (2021).
34. Lee, G. et al. Piezoelectric energy harvesting using mechanical metamaterials and phononic crystals. *Commun. Phys.* **5**, 1–16 (2022).
35. Gururaja, T. R. et al. Piezoelectric composite materials for ultrasonic transducer applications: II. Evaluation of ultrasonic medical applications. *IEEE Trans. Sonics Ultrason.* **32**, 499–513 (1985).
36. Kim, T. et al. Flexible 1–3 composite ultrasound transducers with silver-nanowire-based stretchable electrodes. *IEEE Trans. Ind. Electron.* **67**, 6955–6962 (2020).
37. Sun, P. et al. High frequency PMN-PT 1-3 composite transducer for ultrasonic imaging application. *Ferroelectrics* **408**, 120–128 (2010).
38. Smith, W. A. et al. Modeling 1-3 composite piezoelectrics: thickness-mode oscillations. *IEEE Trans. Ultrason. Ferroelectr. Freq. Control* **38**, 40–47 (1991).
39. Desilets, C. S. et al. The design of efficient broad-band piezoelectric transducers. *IEEE Trans. Sonics Ultrason.* **25**, 115–125 (1978).
40. Grewe, M. G. et al. Acoustic properties of particle/polymer composites for ultrasonic transducer backing applications. *IEEE Trans. Ultrason. Ferroelectr. Freq. Control.* **37**, 506–514 (1990).
41. Larmagnac, A. et al. Stretchable electronics based on Ag-PDMS composites. *Sci. Rep.* **4**, 7254 (2014).
42. Hou, C. et al. Optimized backing layers design for high frequency broad bandwidth ultrasonic transducer. *IEEE Trans. Biomed. Eng.* **69**, 475–481 (2022).
43. Walker, E. L., Jin, Y., Reyes, D. & Neogi, A. Sub-wavelength lateral detection of tissue-approximating masses using an ultrasonic metamaterial lens. *Nat. Commun.* **11**, 5967 (2020).
44. Li, Z. et al. Acoustic hole-hologram for ultrasonic focusing with high sensitivity. *IEEE Sens. J.* **21**, 8935–8942 (2021).
45. Fan, S.-W. et al. Acoustic vortices with high-order orbital angular momentum by a continuously tunable metasurface. *Appl. Phys. Lett* **116**, 16 (2020).
46. Baudoin, M. et al. Spatially selective manipulation of cells with single-beam acoustical tweezers. *Nat. Commun.* **11**, 4244 (2020).
47. Chen, D. et al. An optimization design strategy of 1–3 piezocomposite ultrasonic transducer for imaging applications. *Mater. Today Commun.* **24**, 100991 (2020).
48. Culjat, M. O., Goldenberg, D., Tewari, P. & Singh, R. S. A review of tissue substitutes for ultrasound imaging. *Ultrasound Med. Biol.* **36**, 861–873 (2010).

Acknowledgements

This work was supported by the National Natural Science Foundations of China under Grant 61974110 and Grant 62104177; in part by the Fundamental Research Funds for the Central Universities under Grant YJSJ23019, Grant QTZX23022, and Grant JBF211103; in part by the China Postdoctoral Science Foundation(No: 2023M732745); in part by the Shaanxi Provincial Association of Science and Technology Young Talents Support Project under Grant 20190105; and in part by the Xijiang Innovation Team Introduction Program of Zhaoqing, the Industry-University-Academy Cooperation Program of Xidian University-Chongqing IC Innovation Research Institute, under Grant CQIRI-2021CXY-Z03.

Author contributions

C.H.: Methodology, Writing, Visualization. Z.L.: Conceptualization, Software, Data curation. C.F.: Methodology, Funding acquisition. Y.L.: Validation. Y.W.: Methodology, Software. T.Z.: Methodology. Y.Q.: Resources. D.C.: Writing. X.L.: Supervision. W.B.: Supervision. Y.Y.: Funding acquisition, Supervision.

Competing interests

The authors declare no competing interests.

Additional information

Supplementary information The online version contains supplementary material available at https://doi.org/10.1038/s42005-023-01361-3.

Correspondence and requests for materials should be addressed to Chunlong Fei or Yintang Yang.

Peer review information *Communications Physics* thanks the anonymous reviewers for their contribution to the peer review of this work.

Reprints and permission information is available at http://www.nature.com/reprints

Publisher's note Springer Nature remains neutral with regard to jurisdictional claims in published maps and institutional affiliations.